



Weak bosons as partons below 10 TeV partonic center-of-momentum

Innes Bigaran ^{1,2,*} and Richard Ruiz ^{3,†}¹*Department of Physics & Astronomy, Northwestern University, 2145 Sheridan Road, Evanston, IL 60208, USA*²*Theoretical Physics Department, Fermilab, P.O. Box 500, Batavia, IL 60510, USA*³*Institute of Nuclear Physics – Polish Academy of Sciences (IFJ PAN), ul. Radzikowskiego, Kraków, 31-342, Poland*

(Dated: February 13, 2025)

We investigate the modeling of weak boson number densities for leptons and hadrons in practical calculations in the Standard Model. Working in the framework of the Effective W Approximation (EWA) and in R_ξ and axial gauges, we derive the unrenormalized, tree-level parton number density functions for weak bosons from massless leptons at next-to-leading power in the collinear expansion. Corrections exhibit a number of properties, including those conjectured but never universally derived. Parallels with heavy quark factorization are also found. We avoid pathologies through a novel set of kinematical consistency conditions. When satisfied, good agreement between the full and approximated matrix elements is achieved. Findings suggest that the EWA may be testable at the Large Hadron Collider with $\mathcal{L} = 450 \text{ fb}^{-1}$ of same-sign WW scattering data at $\sqrt{s} = 13.6 \text{ TeV}$.

Introduction: Protons (p) and neutrons make up all stable matter in the visible universe; they constitute the core of atoms and the fuel for stars. Beyond these broad connections, it is also interesting to study hadronic structure in its own right, as a laboratory for quantum field theories and the interplay among gauge structures in the Standard Model (SM) of particle physics.

Despite color confinement in quantum chromodynamics (QCD), it is still possible to reliably describe hadronic structure with the QCD-improved parton model. A core tenet is the existence of “sea” partons, i.e., a near continuum of low-energy gluons and light quark-antiquark pairs in a hadron. Importantly, sea partons originate from higher energy “valance” quarks that radiate gluons, which can subsequently split and populate sea states.

In multi-TeV pp collisions, like those at the Large Hadron Collider (LHC), hard partonic scattering scales Q can be *much* larger than the masses of heavy-flavored quarks. Under such circumstances, the parton sea can be extended to include perturbatively generated charm quarks [1], bottom quarks [2, 3], and even top quarks [4, 5]. Since (valence) quarks carry electric charges and can emit photons, the sea distributions of the proton [6–8] and neutron [6, 9] also have photon components.

In the SM, quarks (q) and leptons (ℓ) carry weak gauge charges, and the emergence of (perturbatively generated) W and Z bosons as sea partons in ultra high-energy pp , $\ell\ell$, and ℓp collisions has long been a qualitative prediction of the SM [10–12]. However, what practically constitutes “ultra high energies” has never been firmly established.

In this work, we find that the answer is about 800 GeV. More specifically, when an incoming fermion radiates a collinear W with at least $E_V = 800 \text{ GeV}$ of energy (900 GeV for Z) in the partonic center-of-momentum

(pCM) frame, the partonic description of *weak bosons* becomes a reliable approximation of full matrix elements.

Presently, there is no all-orders collinear factorization theorem that extends the parton model to the electroweak (EW) sector. It is unclear whether such a formulation is even possible due to the Bloch-Nordsieck Theorem and other obstacles [13–24]. Historically, predictions for EW boson parton number density functions (PDFs) have varied significantly [12, 25–31]. Only recently have kinematical regimes been identified where lowest order (LO) predictions for W/Z PDFs may be reliable [31–35], which we can now more firmly and broadly establish.

Even at LO, reliable predictions for weak boson PDFs can have an impact. LHC data, for example, shows that the same-sign WW scattering signal process, $W_1^\pm W_2^\pm \rightarrow W_3^\pm W_4^\pm \rightarrow \ell^\pm \ell'^\pm \nu_\ell \nu_{\ell'}$ is well-described by LO matrix elements [36–42]. It would be appealing if LO predictions for W/Z PDFs of a proton could broadly describe LHC data. Among applications, one could more easily conceptualize and quantify the impact of new physics [41, 43, 44], in analogy to heavy quark PDFs [4, 5, 45, 46]. Regardless of impact, a full and complete understanding of EW symmetry breaking necessitates the study and measurement of EW boson PDFs.

We report progress of this agenda. In the context of the Effective W Approximation (EWA) [10–12], and in multiple gauges, we present expressions for the unrenormalized, tree-level PDFs for helicity-polarized weak bosons in massless, chiral leptons at next-to-leading power (NLP) in the collinear expansion. The NLP corrections are process-independent, exhibit phenomenologically interesting properties, and can reconcile previous findings. Importantly, preservation of (i) the collinear approximation, (ii) gauge invariance, and (iii) positive-definiteness results in a set of kinematic consistency conditions that have not been previously reported. Conditions can be satisfied at the LHC, meaning that it may be possible to measure the W and Z content of the proton at the LHC with the $\mathcal{L} \sim \mathcal{O}(500) \text{ fb}^{-1}$ of Run III data.

* ibigaran@fnal.gov† rruiz@ifj.edu.pl

The outline of this work is as follows. We first summarize our theoretical framework, the organization of our calculation, and report our NLP-accurate PDFs. We then discuss the phenomenological implications of our results, and illustrate findings in the context of a $\sqrt{s} = 5$ TeV lepton collider. We conclude with outlook for testing the EWA at the LHC.

Setup: We start by considering the high-energy, muon-hadron deep-inelastic scattering (DIS) process

$$\mu^-(p_i) + h(k) \xrightarrow{V_\lambda h \rightarrow X} \ell(p_f) + X(k'), \quad (1)$$

where $\ell \in \{\mu^-, \nu_\mu\}$, mediated by the exchange boson $V \in \{W^\pm, Z\}$ with helicity $\lambda \in \{\pm 1, 0, S\}$, momentum $q = p_i - p_f$, and squared virtuality $q^2 \equiv -Q^2 < 0$. Throughout this work we take $\sqrt{Q^2} \gtrsim \mathcal{O}(M_V)$.

We assume the following momentum assignments:

$$p_i^\mu = E_i (1, 0, 0, +1), \quad (2a)$$

$$p_f^\mu = \left((1-z)E_i, \vec{p}_T, \sqrt{(1-z)^2 E_i^2 - p_T^2} \right) \quad (2b)$$

$$\equiv (1-z)E_i (1, \sin \theta_\ell \cos \phi_\ell, \sin \theta_\ell \sin \phi_\ell, \cos \theta_\ell),$$

$$q^\mu = p_i^\mu - p_f^\mu \equiv \quad (2c)$$

$$\left(zE_i, |\vec{q}| \sin \theta_V \cos \phi_V, |\vec{q}| \sin \theta_V \sin \phi_V, |\vec{q}| \cos \theta_V \right).$$

Here, $z = E_V/E_i$ is the fraction of energy V carries from μ . Under these assignments both leptons are massless, with $p_i^2 = p_f^2 = 0$. From momentum conservation one can derive exact relationships between (θ_ℓ, ϕ_ℓ) and (θ_V, ϕ_V) .

To build our helicity-polarized PDFs, we use the following basis of polarization vectors for V_λ with mass M_V and virtuality $\sqrt{q^2}$ in a general R_ξ gauge:

$$\varepsilon^\mu(q, \lambda = \pm 1) = \frac{1}{\sqrt{2}} \left(0, -\lambda \cos \theta_V \cos \phi_V + i \sin \phi_V, \right. \\ \left. -\lambda \cos \theta_V \sin \phi_V - i \cos \phi_V, \lambda \sin \theta_V \right), \quad (3a)$$

$$\varepsilon^\mu(q, \lambda = 0) = \frac{E_V}{\sqrt{q^2} |\vec{q}|} \left(\frac{|\vec{q}|^2}{E_V}, q_x, q_y, q_z \right) \quad (3b)$$

$$= \frac{q^\mu}{\sqrt{q^2}} + \tilde{\varepsilon}_0^\mu(q), \quad \text{where} \quad (3c)$$

$$\tilde{\varepsilon}_0^\mu(q) \equiv \frac{\sqrt{q^2}}{(E_V + |\vec{q}|) |\vec{q}|} (-1, q_x, q_y, q_z), \quad (3d)$$

$$\varepsilon^\mu(q, \lambda = S) = \sqrt{\frac{1}{q^2} + \frac{(\xi - 1)}{q^2 - \xi M_V^2}} q^\mu. \quad (3e)$$

Here, ξ is the gauge-fixing parameter, and the unitary gauge corresponds to taking $\xi \rightarrow \infty$. These polarization vectors obey the completeness relationship

$$\sum_{\lambda=\pm} \varepsilon_\mu(q, \lambda) \varepsilon_\nu^*(q, \lambda) + \varepsilon_\mu(q, 0) \varepsilon_\nu(q, 0) - \varepsilon_\mu(q, S) \varepsilon_\nu(q, S) \\ = -g_{\mu\nu} - \frac{(\xi - 1)}{(q^2 - \xi M_V^2)} q_\mu q_\nu. \quad (4)$$

Vertex	\tilde{g}	g_R^f	g_L^f
$W - f - f'$	$\frac{g}{\sqrt{2}}$	0	1
$Z - f - f$	$\frac{g}{\cos \theta_W}$	$-Q^f \sin^2 \theta_W$	$(T_3^f)_L - Q^f \sin^2 \theta_W$

TABLE I. Coupling definitions for fermions f, f' with weak isospin charge $(T_3^f)_L = \pm 1/2$ and electric charge Q^f .

Following Ref. [10], we decompose the longitudinal polarization vector in Eq. (3b) into its Goldstone component $q^\mu/\sqrt{q^2}$, and gauge component $\tilde{\varepsilon}_0^\mu(q)$. This decomposition makes manifest the decoupling of Goldstone modes in $\mu \rightarrow V_\lambda \ell$ splitting with massless fermions [47]. More explicitly, the contraction of V 's momentum q^μ with the $\mu \rightarrow \ell$ current ($J_{\ell \leftarrow \mu}^\mu$) vanishes, i.e., $q \cdot J_{\ell \leftarrow \mu} = 0$, due to EW current conservation. Similarly, the scalar polarization ($\lambda = S$) decouples since $\varepsilon^\mu(q, S) \propto q^\mu$. Consequently, our results will hold for any ξ .

We make the standard quasi-on-shell approximation [10], and use the longitudinal polarization vector for an on-shell state. This is obtained by making the replacement $1/\sqrt{q^2} \rightarrow 1/M_V$ in Eqs. (3b)-(3d), but nowhere else. The impact of this approximation has been previously explored [27, 48], and will be revisited shortly.

Beyond leading log: We proceed by computing the tree-level helicity amplitudes for $\mu \rightarrow V_\lambda \ell$ splitting. Next, we expand squared amplitudes to leading power (LP) and NLP in θ_ℓ . (In standard references, e.g., Ref. [49], amplitudes are evaluated *after* Taylor expanding.) For $\lambda = 0$, only the leading $\mathcal{O}(M_V^2/E_V^2)$ term is kept. We then integrate over the phase space of ℓ . Formally, the integral over $q^2 \sim \mathcal{O}(p_T^2)$ is ultraviolet divergent, and so we introduce a regulator $\mu_f > 0$ with mass dimension one. Alternatively, one can use dimensional regularization [12].

At LP in the collinear expansion, the tree-level helicity-polarized W/Z PDFs for chiral leptons are

$$f_{V_+/\ell_L}^{\text{LP}}(z, \mu_f^2) = \frac{\tilde{g}^2}{4\pi^2} \frac{g_L^2(1-z)^2}{2z} \\ \left[\log \left(\frac{\mu_f^2 + M_V^2}{M_V^2} \right) - \left(\frac{\mu_f^2}{\mu_f^2 + M_V^2} \right) \right], \quad (5a)$$

$$f_{V_-/\ell_L}^{\text{LP}}(z, \mu_f^2) = \frac{\tilde{g}^2}{4\pi^2} \frac{g_L^2}{2z} \\ \left[\log \left(\frac{\mu_f^2 + M_V^2}{M_V^2} \right) - \left(\frac{\mu_f^2}{\mu_f^2 + M_V^2} \right) \right], \quad (5b)$$

$$f_{V_0/\ell_L}^{\text{LP}}(z, \mu_f^2) = \frac{\tilde{g}^2}{4\pi^2} \frac{g_L^2(1-z)}{z} \left(\frac{\mu_f^2}{\mu_f^2 + M_V^2} \right), \quad (5c)$$

$$f_{V_\lambda/\ell_R}^{\text{LP}}(z, \mu_f^2) = \left(\frac{g_R}{g_L} \right)^2 \times f_{V_{-\lambda}/\ell_L}^{\text{LP}}(z, \mu_f^2), \quad (5d)$$

where the couplings are defined in Table I. Keeping the leading $\mathcal{O}(\mu_f^2/M_V^2)$ terms when $\mu_f^2 \gg M_V^2$ in Eq. (5) recovers the usual expressions in the leading log approximation (LLA) [10–12]. The relationship between LLA,

$$\mu^-(p_i) \rightarrow \ell(p_f) + V_\lambda(q) = \underbrace{\text{LLA} + \mathcal{O}\left(\frac{M_V^2}{\mu_f^2}\right)}_{\text{LP in } \theta_\ell} + \underbrace{\mathcal{O}\left(\frac{\mu_f^2}{E_V^2}, \frac{M_V^2}{E_V^2}\right)}_{\text{NLP in } \theta_\ell} + \dots$$

FIG. 1. Schematic relationship between the leading log (LLA), leading power (LP), and next-to-leading power (NLP) approximations in collinear $\mu^- \rightarrow \ell V_\lambda$ splitting at high energies.

LP, and NLP expansions is illustrated in Fig. 1.

At NLP in the collinear expansion, we obtain:

$$f_{V_+/\ell_L}^{\text{NLP}}(z, \mu_f^2) = f_{V_+/\ell_L}^{\text{LP}}(z, \mu_f^2) \left[1 + \frac{(2-z)M_V^2}{(1-z)E_V^2} \right] - \frac{\mu_f^2}{4E_V^2} (2-z) f_{V_0/\ell_L}^{\text{LP}}(z, \mu_f^2) \quad (6a)$$

$$f_{V_-/\ell_L}^{\text{NLP}}(z, \mu_f^2) = f_{V_-/\ell_L}^{\text{LP}}(z, \mu_f^2) \left[1 + (2-z)\frac{M_V^2}{E_V^2} \right] - \frac{\mu_f^2}{4E_V^2} \frac{(2-z)}{(1-z)} f_{V_0/\ell_L}^{\text{LP}}(z, \mu_f^2), \quad (6b)$$

$$f_{V_0/\ell_L}^{\text{NLP}}(z, \mu_f^2) = f_{V_0/\ell_L}^{\text{LP}}(z, \mu_f^2) - \frac{M_V^2}{2E_V^2} \left[f_{V_+/\ell_L}^{\text{LP}}(z, \mu_f^2) + f_{V_-/\ell_L}^{\text{LP}}(z, \mu_f^2) \right], \quad (6c)$$

$$f_{V_\lambda/\ell_R}^{\text{NLP}}(z, \mu_f^2) = \left(\frac{g_R}{g_L} \right)^2 \times f_{V_{-\lambda}/\ell_L}^{\text{NLP}}(z, \mu_f^2). \quad (6d)$$

For quarks, weak boson PDFs at LLA, LP, and NLP are the same as above, up to precise values of gauge quantum number. In the absence of EW renormalization-group evolution (RGE), as is the case here, weak boson PDFs for hadrons can be obtained through a one-step PDF convolution with standard quark QCD PDFs [10].

Several comments are in order: (i) NLP PDFs can be expressed in terms of LP PDFs of multiple helicities. We interpret this as a manifestation of helicity inversion. (ii) NLP corrections for $\lambda = \pm 1$ grow negative with increasing μ_f^2/E_V^2 . Thus if μ_f is too large, then PDFs will run negative, violating positive-definiteness of LO PDFs. Notably, $\mu_f \ll E_V$ is contrary to the standard practice of setting $\mu_f \sim \mathcal{O}(E_V)$, which is justifiable when EW PDFs are resummed, e.g., Refs. [12, 16, 21, 23], and μ_f is an RGE scale. Here we have $\mu_f/E_V \sim p_T^V/p_z^V \sim \theta_V$, and a breakdown occurs when momenta are taken outside the collinear limit. (iii) NLP corrections for $\lambda = 0$ grow negative with decreasing E_V^2/M_V^2 , which reflects a violation of the on-shell condition $E_V = zE_\ell > M_V$. Once again, restricting $z = E_V/E_\ell > M_V/E_\ell$ is not a standard assumption in applications of the EWA despite the $\mathcal{O}(M_V^2/E_V^2)$ expansion in the derivation of f_{V_0} at LLA.

Note that $\mathcal{O}(M_V^2/E_V^2)$ and $\mathcal{O}(\mu_f^2/E_V^2)$ terms in Eq. (6) violate scaling in the Bjorken sense. In the DIS limit, where E_V and $Q^2 \sim \mu_f^2 \gtrsim M_V^2$ are large but $z \propto Q^2/E_V$ is fixed, $\mathcal{O}(\mu_f^2/E_V^2)$ terms vanish and scaling is recovered. We draw further comparison to heavy quark PDFs, where

quark masses (m_Q) violate scaling (“slow rescaling”) at $\mathcal{O}(m_Q^2/Q^2)$ but vanish in the DIS limit [2, 50, 51].

Corrections to unrenormalized W/Z PDFs beyond LP have been estimated numerically and/or semi-analytically for specific processes [25, 27, 28, 31, 32, 35, 48, 52, 53], albeit with mixed conclusions. For the photon PDF of the electron, corrections beyond the LLA are well-known [54]. To our knowledge, the PDFs in Eq. (6) have not been previously reported. Beyond conventional differences for EWA PDFs [35], we find that many past works have taken inappropriate values of z and μ_f .

To check gauge dependence, we use the 4-dimensional axial gauge of the EW sector [55] with a reference vector $n^\mu = (1, 0, 0, 0)$. Since Goldstone modes decouple in our work, we do not employ the “5-d” formulation as in Refs. [12, 32, 56–58]. In the axial gauge, the $\lambda = \pm 1$ polarization vectors are the same as in the R_ξ gauge. Imposing, the quasi-on-shell condition, the $\lambda = S$ polarization vector is $\varepsilon^\mu(q, \lambda = S) = 0$. For $\lambda = 0$ we have

$$\varepsilon^\mu(q, \lambda = 0) = \frac{1}{\sqrt{(q \cdot n)^2 - n^2 M_V^2}} \left[\frac{M_V n^2}{(q \cdot n)} q^\mu - M_V n^\mu \right]. \quad (7)$$

Polarization vectors satisfy the completeness relationship

$$\sum_{\lambda=\pm} \varepsilon_\mu(q, \lambda) \varepsilon_\nu^*(q, \lambda) + \varepsilon_\mu(q, 0) \varepsilon_\nu(q, 0) - \varepsilon_\mu(q, S) \varepsilon_\nu(q, S) = -g_{\mu\nu} + \frac{n_\mu q_\nu + n_\nu q_\mu}{(n \cdot q)} - \frac{n^2}{(q \cdot n)^2} q_\mu q_\nu. \quad (8)$$

In the axial gauge, the W/Z PDFs at LP and LLA are the same as in the unitary/ R_ξ gauge for all helicities. This is in agreement with Refs. [12, 32]. At NLP, only the transverse PDFs ($\lambda = \pm 1$) are the same in both gauges. For the longitudinal PDF ($\lambda = 0$) at NLP, we obtain

$$f_{V_0/\ell_L}^{\text{NLP}}(z, \mu_f^2) \Big|_{\text{axial}} = f_{V_0/\ell_L}^{\text{LP}}(z, \mu_f^2) - \frac{M_V^2}{2E_V^2} \left[f_{V_+/\ell_L}^{\text{LP}}(z, \mu_f^2) - (1-2z) f_{V_-/\ell_L}^{\text{LP}}(z, \mu_f^2) \right], \quad (9)$$

which differs from Eq. (6c). The breakdown of gauge invariance has two possible sources: (i) neglecting polarization interference, which is conjectured to scale as $\delta f_{\text{Int.}} \sim \mathcal{O}(M_V/E)$ [10], and (ii) imposing the on-shell criterion for the $\lambda = 0$ polarization vector, which is also conjectured to scale as $\delta f_{\text{on-shell}} \sim \mathcal{O}(M_V/E)$ [27]. The

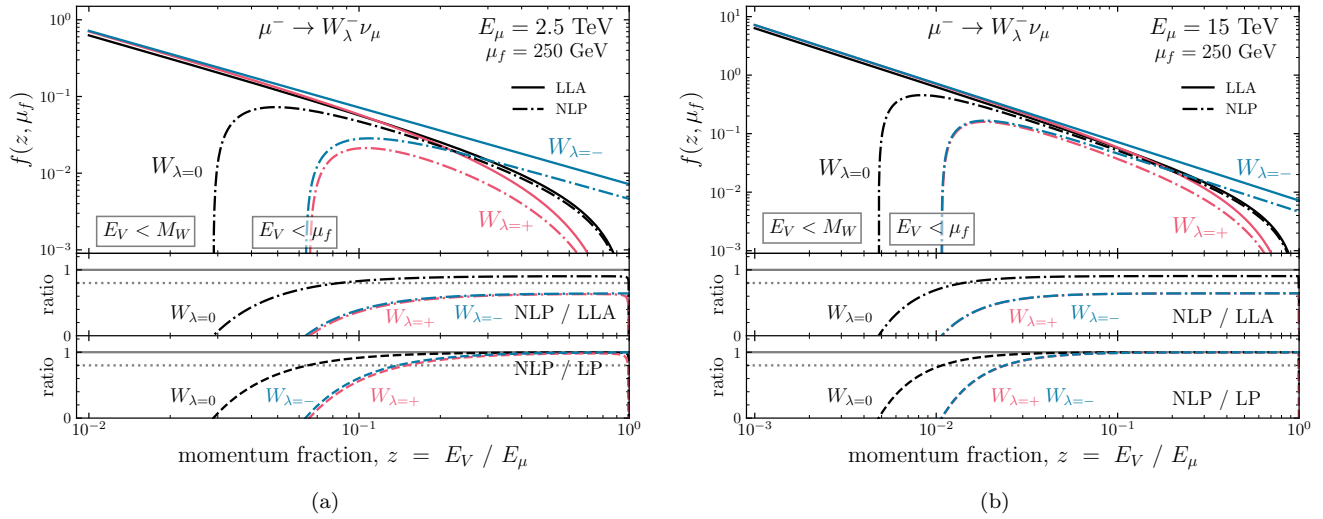


FIG. 2. Upper panel: For (a) $E_\mu = 2.5$ TeV and (b) $E_\mu = 15$ TeV, the NLP (dash-dot) and LLA (solid) PDFs for W in $\mu^- \rightarrow W_\lambda^- \nu_\mu$, as a function $z = E_V/E_\mu$ with $\mu_f = 250$ GeV. Middle (Bottom) panel: ratio of NLP and LLA (LP) PDFs.

takeaway is that EWA predictions can be trusted only when NLP corrections are negligible, i.e., $(M_W^2/E_V^2) \ll 1$ and $(\mu_f^2/E_V^2) \ll 1$. This is a key finding of our work.

To illustrate the impact of these kinematic criteria on weak boson PDFs, we show in the upper panels of Figs. 2(a) and 2(b) the NLP (dash-dot) and LLA (solid) PDFs for W in $\mu^- \rightarrow W_\lambda^- \nu_\mu$ splitting as a function of energy fraction $z = E_W/E_\mu$, with a cutoff scale of $\mu_f = 250$ GeV, for (a) $E_\mu = 2.5$ TeV and (b) $E_\mu = 15$ TeV. The two energy configurations correspond, respectively, to an LHC-like valance parton for $\sqrt{s} = 13 - 14$ TeV, and a benchmark configuration for a $\sqrt{s} = 30$ TeV $\mu^+\mu^-$ collider [59–61]. In the lower panels, we show the NLP-to-LLA (middle) and NLP-to-LP (bottom) PDF ratios.

Qualitatively, one sees pathological behaviors emerge as $z \rightarrow 0$. Specifically, the $\lambda = 0$ ($\lambda = \pm 1$) PDF at NLP goes negative for $E_V < M_W$ ($E_V < \mu_f$). Importantly, as shown in the bottom panels, pure NLP corrections quickly become negligible when E_V surpasses μ_f . This means that for moderate and large z , the NLP-to-LLA ratio in the middle panels can be interpreted as the LP-to-LLA ratio. For fixed μ_f , the LP-to-LLA ratio is actually independent of z . Since we choose $\mu_f = 250$ GeV $\gtrsim \mathcal{O}(M_W)$, we are not in the large-log limit, and so-called $\mathcal{O}(1)$ terms at LP are relevant at the $\delta f^{\text{LP}}/f^{\text{LLA}} \sim +10\%$ (-35%) level for $\lambda = 0$ ($\lambda = \pm 1$).

EWA in high-energy lepton collisions: As a final illustration of our work, we consider the scattering processes

$$W_0^+ W_0^- \rightarrow hh \quad \text{and} \quad W_T^+ W_T^- \rightarrow \gamma\gamma, \quad (10)$$

at LO in $e^+\mu^-$ collisions at $\sqrt{s} = 5$ TeV, again to represent pCM scales already accessible at the LHC. T denotes any transverse ($\lambda = \pm 1$) helicity. We focus on these processes because their matrix elements (MEs) are mediated almost exclusively by longitudinal-longitudinal and

transverse-transverse WW scattering [35, 62]. Cross sections at the integrated (σ) and differential ($d\sigma$) level are obtained assuming the following factorization formula

$$\sigma_{e^+\mu^- \rightarrow \mathcal{F}+X} = f_{W_\lambda^+/e^+} \otimes f_{W_\lambda^-/\mu^-} \otimes \hat{\sigma}_{W_\lambda^+ W_\lambda^- \rightarrow \mathcal{F}}. \quad (11)$$

Here, $\hat{\sigma}$ is the “parton-level” cross section for the processes in Eq. (10), and \otimes denotes a convolution over z_i for incoming W boson i . Unless noted otherwise, we require $z_{1(2)} > z_{\min} = (M_W/E_{e(\mu)})$ for all EWA channels.

To build and evaluate our MEs, we have implemented the helicity-polarized LP [Eq. (5)] and NLP [Eq. (6)] PDFs for W and Z bosons in electrons and muons into a forthcoming release of the simulation framework MadGraph5_aMC@NLO [35, 62–64]. Initial-state W ’s are assumed collinear to the beam and on-shell, with $M_W^2 \neq 0$. Helicities and energies are defined in the frame of the (WW) -system. To regulate the 3γ ME, we require

$$p_T^\gamma > 150 \text{ GeV}, \quad |\eta^\gamma| < 3, \quad \text{and} \quad \Delta R(\gamma, \gamma) > 0.4. \quad (12)$$

Since we consider only $\sqrt{s} = 5$ TeV, the phase space requirements above are sufficient to ensure our MEs are well-defined in the CSS sense [65]. However, this is not guaranteed for larger \sqrt{s} or alternative processes [23]. We set $\mu_f = 250$ GeV (450 GeV) for the $WW \rightarrow hh$ ($\gamma\gamma\gamma$), which is approximately the threshold scale. For all other inputs, we follow Ref. [35]. For non-EWA processes, MEs are computed using all interfering diagrams.

In the upper panel of Fig. 3(a) we show the invariant mass distribution of the (hh) -system in $W_0^+ W_0^- \rightarrow hh$ scattering as predicted by the EWA at LLA (dot-dashed), LP (dotted), and NLP (dashed), as well as by the full $2 \rightarrow 4$ ME for $e^+\mu^- \rightarrow \bar{\nu}_e \nu_\mu hh$ (solid). For comparison, we also include EWA predictions at LLA without the $E_V > M_V$ requirement [c.f., Ref. [35]] (dashed). In the

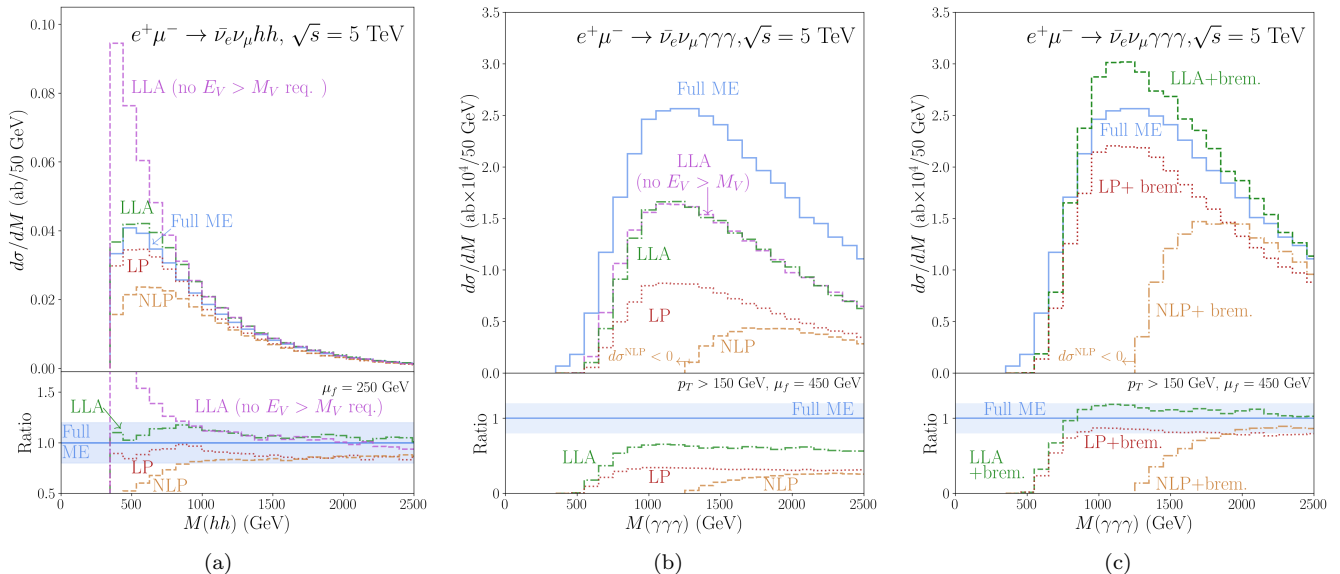


FIG. 3. (a) Upper: The invariant mass distribution of the (hh) -system in the $W_0^+ W_0^- \rightarrow hh$ scattering process at LLA [without imposing $E_V > M_V$] (dashed), LLA (dotdashed), LP (dotted), and NLP (dashed), along with the full $2 \rightarrow 4$ ME (solid) in $e^+ \mu^-$ collisions at $\sqrt{s} = 5 \text{ TeV}$. Lower: ratios with respect to the full ME. (b) Same as (a) but for the (3γ) -system in the $W_T^+ W_T^- \rightarrow 3\gamma$ scattering process and the full $2 \rightarrow 5$ ME. (c) Same as (b) but with the “bremsstrahlung” factor (r_{brem}).

lower panel we show the ratios with respect to the full ME along with a tolerance band of $\pm 20\%$ around unity.

We begin by noting the agreement between the full ME, LLA, and LP distributions over the entire invariant mass range. For all curves, disagreements with the full ME fall below $\mathcal{O}(\pm 20\%)$ for $M(hh) = M(WW) \gtrsim 1 \text{ TeV}$ and further improve at larger $M(WW)$. For low $M(WW)$, and hence low z_i , NLP predictions are far below the full ME. However, the NLP and LP predictions converge for $M(WW) \gtrsim 1.6 \text{ TeV}$, which corresponds to $E_W \sim 800 \text{ GeV}$ and $(M_W^2/E_W^2) \sim \mathcal{O}(1\%)$. The impact of relaxing the $E_V > M_V$ requirement is stark and leads to an overestimation of the low- $M(WW)$ phase space.

For $M(hh) > 2m_h$ (1.6 TeV), cross sections [fb] with standard 3-point scale uncertainties [%] are given in Table II. Also shown are the deviations from the full ME [%]. In summary, the LLA prediction best recovers the full ME at large $M(WW)$ but with an unrealistic $\mathcal{O}(1\%)$ uncertainty. LP and NLP predictions feature slightly worse agreements but with more reliable uncertainties. It is also remarkable that setting $\mu_f = 4m_h \sim 500 \text{ GeV}$, which would reconcile (N)LP and full ME predictions, is roughly at the maximum of the $M(WW)$ distribution.

In Fig. 3(b) we show the same information as in Fig. 3(a) but for the $W_T^+ W_T^- \rightarrow \gamma\gamma\gamma$ process and the full $2 \rightarrow 5$ ME for $e^+ \mu^- \rightarrow \bar{\nu}_e \nu_\mu \gamma\gamma\gamma$. We find no impact of the $E_V > M_V$ requirement and will not discuss it here further. Immediately, one notices that all EWA predictions underestimate the full ME by at least $\mathcal{O}(30\%)$.

The reason for the disagreement is that the $W_T W_T \rightarrow 3\gamma$ process is actually a poor toy process for modeling the EWA at $\sqrt{s} = 5 \text{ TeV}$. The full ME consists of four classes

of diagrams: (i-iii) $WW \rightarrow 3\gamma + 0$ -2 bremsstrahlung and (iv) single- W exchange + 3 bremsstrahlung. The EWA captures only class (i) and the phase space requirements of Eq. (12) are insufficient to suppress the other classes.

To demonstrate this, we consider the full matrix element for the $2 \rightarrow 4$ process $e^+ \mu^- \rightarrow \bar{\nu}_e \nu_\mu \gamma\gamma$. We estimate the bremsstrahlung contribution to the full (3γ) ME by scaling the (2γ) rate by a QED Sudakov factor:

$$\sigma_{3\gamma}^{\text{brem.}} = \mathcal{S}_{\text{QED}} \times \sigma^{\text{Full}}(e^+ \mu^- \rightarrow \bar{\nu}_e \nu_\mu \gamma\gamma), \quad (13a)$$

$$\mathcal{S}_{\text{QED}} = \frac{\alpha}{4\pi} \log^2 \left(\frac{\mu_S^2}{(p_T^\gamma)^2} \right). \quad (13b)$$

For $\sigma^{\text{Full}}(2\gamma)$, we impose Eq. (12), and set $(p_T^\gamma, \mu_S) = (150 \text{ GeV}, 450 \text{ GeV})$ in \mathcal{S}_{QED} . EWA rates are then augmented by a “bremsstrahlung” factor ($r_{\text{brem.}}$) defined by

$$\sigma_{3\gamma}^{\text{EWA+brem.}} = \sigma_{3\gamma}^{\text{EWA}} + \sigma_{3\gamma}^{\text{brem.}} \quad (14)$$

$$\equiv \sigma_{3\gamma}^{\text{EWA}} \times (1 + r_{\text{brem.}}). \quad (15)$$

The value of $r_{\text{brem.}}$ depends on the accuracy of σ^{EWA} . For the NLP channel, $\mathcal{O}(\mu_f^2/E_V^2)$ corrections drive $\sigma_{3\gamma}^{\text{NLP}}$ negative when $M(\gamma\gamma) \lesssim 1250 \text{ GeV}$. Therefore, for this channel we additionally require $M(\gamma\gamma) > 1100 \text{ GeV}$ when computing $\sigma^{\text{Full}}(2\gamma)$ and apply the bremsstrahlung correction to $\sigma_{3\gamma}^{\text{EWA}}$ only for $M(\gamma\gamma) \gtrsim 1250 \text{ GeV}$.

In Fig. 3(c), we show the same information as in Fig. 3(b) but with EWA rates scaled as in Eq. (15). In doing so, we obtain reasonable agreement between predictions for the EWA and the full ME. Predictions for LLA+brem. and LP+brem. fall within $\mathcal{O}(\pm 20\%)$ of the

	$M(hh) > 2m_h$ (1.6 TeV)	$(\sigma^{\text{Full}} - \sigma^{\text{EWA}})/\sigma^{\text{Full}}$
σ^{Full} [fb]	1.66 (0.186)	- (-)
σ^{LLA} [fb]	$1.86^{+3\%}_{-1\%}$ $\left(0.194^{+1\%}_{<-0.5\%}\right)$	+12% (+4%)
σ^{LP} [fb]	$1.51^{+18\%}_{-40\%}$ $\left(0.158^{+16\%}_{-39\%}\right)$	-9% (-14%)
σ^{NLP} [fb]	$1.16^{+0\%}_{-29\%}$ $\left(0.157^{+15\%}_{-39\%}\right)$	-30% (-16%)

TABLE II. Predicted cross sections (σ) [fb] for $e^+\mu^- \rightarrow \bar{\nu}_e\nu_\mu hh$ at $\sqrt{s} = 5$ TeV using the full ME (row 1) and the EWA at various accuracies (rows 2-4), along with standard 3-point scale uncertainties, for $M(hh) > 2m_h$ (1.6 TeV). Also shown (column 3) are the deviations [%] from the full ME.

full ME for $M(3\gamma) = M(WW) \gtrsim 800$ GeV. Predictions for NLP+brem. reach this threshold at $M(WW) \gtrsim 1.8$ TeV and further improve with increasing $M(WW)$.

We again stress how well a full ME can be approximated with the EWA and a *naïve* choice for μ_f . It is well-known that weak boson PDFs for transverse helicities carry $\mathcal{O}(100\%)$ scale uncertainties; (N)LP corrections do not change this fact. Nevertheless, there are two paths to reduce this ambiguity: (i) multi-leg matching, which was demonstrated in Ref. [35], and (ii) introducing a Sudakov factor into the formula of Eq. (11). When using renormalized PDFs, scale invariance of physical observables guarantees the existence of a Sudakov factor [66]. Even at LO, the impact can be significant [67, 68]. A demonstration, however, is left to future work.

Discussion and conclusion: We report the first NLP-accurate calculation of W/Z PDFs for high-energy fermions in the framework of the EWA. From these PDFs [Eq. (6)], we have derived new kinematical criteria that lead to good agreement between full matrix elements and the EWA. Neglecting these criteria can lead the EWA to significantly overestimate cross sections. As a rule-of-thumb, the collinear approximation, gauge invariance, and positive-definiteness can be preserved by requiring W/Z bosons to carry $E_V > 800 - 900$ GeV of energy (or $10\times$ their masses) in the pCM frame and restricting μ_f to be close to a process' threshold scale.

Given the relative lowness of 800 GeV, it may be possible to test the EWA at the LHC, and hence test the emergence of W bosons as (perturbatively-generated) partons in a proton. At $\sqrt{s} = 13.6$ TeV, the same-sign WW scattering process $pp \rightarrow W^\pm W^\pm jj$ at $\mathcal{O}(\alpha^4)$ has a LO cross section of $\sigma_{\text{LHC}13.6} \sim 5.5$ (1.0) fb with generator-level requirements $M(WW) > 1$ (1.6) TeV and $M(jj) > 500$ GeV. Taking the double $W \rightarrow e/\mu$ branching rate $\text{BR}^2 \approx 4/81$, and assuming realistic [36–39] selection and acceptance rates of $\epsilon \times \mathcal{A} \approx 25\%$, then about $N = \mathcal{L}\sigma\text{BR}^2\epsilon\mathcal{A} \approx 30$ (6) events with $\mathcal{L} = 450 \text{ fb}^{-1}$ are anticipated. While this number is not large, it is large enough to be interesting and motivate further study. Of particular importance is an EWA-compatible parton shower for pp collisions, which is the last missing ingredient for simulating fully exclusive events at the LHC.

ACKNOWLEDGEMENTS

The authors thank A. Apyan, A. Denner, T. Han, S. Lowette, F. Olness, C. Quigg, J. Reuter, G. Pelliccioli, K. Potamianos, and the `mg5amc` team for useful discussions.

This manuscript has been authored in part by Fermi Forward Discovery Group, LLC under Contract No. 89243024CSC000002 with the U.S. Department of Energy, Office of Science, Office of High Energy Physics. The work of I.B. was performed in part at the Aspen Center for Physics, supported by a grant from the Alfred P. Sloan Foundation (G-2024-22395). RR acknowledges the support of Narodowe Centrum Nauki under Grant Nos. 2019/34/E/ST2/00186 and 2023/49/B/ST2/04330 (SNAIL). The authors acknowledge support from the COMETA COST Action CA22130.

Appendix A: Usage in MG5_aMC@NLO

LP and NLP PDFs for helicity-polarized W and Z bosons in electrons and muons is a new feature in the simulation framework `MadGraph5_aMC@NLO` [63, 64]. The development builds on releases for helicity-polarized parton scattering [62] and EWA PDFs at LLA [35].

To access LP and NLP PDFs, nearly identical syntax can be used as introduced in Ref. [35]. The main addition is the `run_card` option `evaorder`. The available values for `evaorder` and their impact are found in Table III.

NLP corrections are only available for weak bosons, not for the photon. LP corrections to PDFs for photons from leptons are available as developed in Ref. [54]. The option `ievo_eva` for setting the EWA evolution variable, as developed in Ref. [35], is available only for LLA PDFs.

The syntax for simulating the $W_0^+W_0^- \rightarrow hh$ process with the EWA at LP, as done in Fig. 3(a), is given by

```
set group_subprocesses false
generate w+{0} w- {0} > h h QED=2 QCD=0
output
launch
analysis=off
set ebeam 10000 # GeV
set nevents 10k
set lpp1 -3 # e+ beam
set lpp2 4 # mu- beam
set pdlabel eva
set evaorder 1 # 0=LLA (default), 1=LP, 2=NLP
set fixed_ren_scale true
set fixed_fac_scale1 true
set fixed_fac_scale2 true
set dsqrt_q2fact1 250
set dsqrt_q2fact2 250
set scalefact 1.0
set no_parton_cut
set use_syst true
done
```

For descriptions of the above syntax, see Refs. [35, 62, 64].

evaorder value [int]	PDF accuracy	Eqs.
0	LLA (default)	Ref. [35]
1	LP	Eq. (5)
2	NLP	Eq. (6)

TABLE III. evaorder settings for MadGraph5_aMC@NLO

Appendix B: Checks against MG5_aMC@NLO

As a check of our implementation of LP [Eq. (5)] and NLP [Eq. (6)] PDFs into mg5amc, we have independently computed the opposite-sign WW scattering process

$$W^+(p_A, \lambda_A) W^-(p_B, \lambda_B) \rightarrow h(p_1) h(p_2). \quad (\text{B1})$$

In the Unitary gauge, the matrix element is

$$-i\mathcal{M}(\lambda_A, \lambda_B) = \sum_{d \in \{s, t, u, 4\}} -i\mathcal{M}_d(\lambda_A, \lambda_B), \quad (\text{B2})$$

where the sum runs over four tree-level graphs. For fixed helicity $\{\lambda_k\}$ and momenta $\{p_k\}$, the sub-amplitudes are

$$-i\mathcal{M}_s = +i \frac{3g^2 m_h^2}{2} \frac{[\varepsilon(p_A, \lambda_A) \cdot \varepsilon(p_B, \lambda_B)]}{Q^2 - m_h^2}, \quad (\text{B3a})$$

$$-i\mathcal{M}_4 = +i \frac{g^2}{2} [\varepsilon(p_A, \lambda_A) \cdot \varepsilon(p_B, \lambda_B)], \quad (\text{B3b})$$

$$-i\mathcal{M}_t = \frac{+ig^2}{t - M_W^2} \left\{ M_W^2 [\varepsilon(p_A, \lambda_A) \cdot \varepsilon(p_B, \lambda_B)] + [\varepsilon(p_A, \lambda_A) \cdot p_1] [\varepsilon(p_B, \lambda_B) \cdot p_2] \right\}, \quad (\text{B3c})$$

$$-i\mathcal{M}_u = \frac{+ig^2}{u - M_W^2} \left\{ M_W^2 [\varepsilon(p_A, \lambda_A) \cdot \varepsilon(p_B, \lambda_B)] + [\varepsilon(p_A, \lambda_A) \cdot p_2] [\varepsilon(p_B, \lambda_B) \cdot p_1] \right\}. \quad (\text{B3d})$$

In the partonic center-of-mass frame, momenta are

$$p_A = \frac{Q}{2} (1, 0, 0, +\beta_W), \quad |\vec{p}_A| = |\vec{p}_B| = \beta_W \frac{Q}{2}, \quad (\text{B4a})$$

$$p_B = \frac{Q}{2} (1, 0, 0, -\beta_W), \quad (\text{B4b})$$

$$p_1 = \frac{Q}{2} (1, \beta_h \sin \theta \sin \phi, \beta_h \sin \theta \cos \phi, \beta_h \cos \theta), \quad (\text{B4c})$$

$$p_2 = \frac{Q}{2} (1, -\vec{p}_1), \quad |\vec{p}_1| = |\vec{p}_2| = \beta_h \frac{Q}{2}. \quad (\text{B4d})$$

These assignments generate the following contractions between polarization vectors (all others vanish):

$$\varepsilon(p_A, \pm 1) \cdot \varepsilon(p_B, \pm 1) = -1, \quad (\text{B5a})$$

$$\varepsilon(p_A, 0) \cdot \varepsilon(p_B, 0) = -1 + \frac{Q^2}{2M_W^2}. \quad (\text{B5b})$$

Similarly, these assignments generate the following contractions between polarization vectors and momenta:

$$\varepsilon(p_A, \pm 1) \cdot p_1 = \pm \frac{e^{\pm i\phi}}{2\sqrt{2}} Q \sqrt{1 - 4r_h} \sin \theta, \quad (\text{B6a})$$

$$\varepsilon(p_A, 0) \cdot p_1 = \frac{Q^2}{4M_W} \left[\sqrt{1 - 4r_W} - \sqrt{1 - 4r_h} \cos \theta \right], \quad (\text{B6b})$$

$$\varepsilon(p_A, \pm 1) \cdot p_2 = -[\varepsilon(p_A, \pm 1) \cdot p_1], \quad (\text{B6c})$$

$$\varepsilon(p_A, 0) \cdot p_2 = \frac{Q^2}{4M_W} \left[\sqrt{1 - 4r_W} + \sqrt{1 - 4r_h} \cos \theta \right], \quad (\text{B6d})$$

$$r_W = \frac{M_W^2}{Q^2}, \quad r_h = \frac{m_h^2}{Q^2}. \quad (\text{B6e})$$

The *helicity-polarized*, parton-level cross sections can then be determined (numerically) from the formula [62]

$$\hat{\sigma}(\lambda_A, \lambda_B) = \int dPS_2 \frac{d\hat{\sigma}(\lambda_A, \lambda_B)}{dPS_2}, \quad \text{where} \quad (\text{B7a})$$

$$\frac{d\hat{\sigma}(\lambda_A, \lambda_B)}{dPS_2} = \frac{1}{2Q^2 \sqrt{1 - 4r_W}} |\mathcal{M}(\lambda_A, \lambda_B)|^2, \quad (\text{B7b})$$

$$dPS_2 = \frac{d \cos \theta d\phi}{2(4\pi)^2} \sqrt{1 - 4r_h}. \quad (\text{B7c})$$

Helicity-polarized cross sections at the level of muons are obtained through the usual PDF convolutions [10]:

$$\sigma_{\lambda_A \lambda_B}(\mu^+ \mu^- \rightarrow hh + X) = f_{W_{\lambda_A}^+ / \mu^+} \otimes f_{W_{\lambda_B}^- / \mu^-} \otimes \hat{\sigma}_{W^+ W^- \rightarrow hh}(\lambda_A, \lambda_B) \quad (\text{B8})$$

$$= \int_{\tau_{\min}}^1 d\tau \int_{\tau}^1 \frac{dz_1}{z_1} f_{W_{\lambda_A}^+ / \mu^+}(z_1, \mu_f) \times f_{W_{\lambda_B}^- / \mu^-}(z_2, \mu_f) \times \hat{\sigma}_{W^+ W^- \rightarrow hh}(\lambda_A, \lambda_B), \quad (\text{B9})$$

$$\text{with } z_2 = \frac{\tau}{z_1} \text{ and } \tau_{\min} = \frac{(2m_h)^2}{s}. \quad (\text{B10})$$

Importantly, we impose the additional threshold condition that $f_{W/\mu}(z_i) = 0$ for $E_{W_i} = z_i \sqrt{s}/2 < M_W$.

Unpolarized cross sections are recovered through averaging over initial-state spin/helicity configurations:

$$\hat{\sigma}_{\text{unpol}} = \frac{1}{3^2} \sum_{\lambda_A, \lambda_B \in \{\pm 1, 0\}} \hat{\sigma}(\lambda_A, \lambda_B), \quad (\text{B11})$$

$$\sigma = \frac{1}{3^2} \sum_{\lambda_A, \lambda_B \in \{\pm 1, 0\}} \sigma_{\lambda_A \lambda_B}. \quad (\text{B12})$$

We summarize our results in Table IV for the following SM and collider inputs

$$g \approx 0.6532, \quad M_W \approx 80.42 \text{ GeV}, \quad m_h = 125 \text{ GeV}, \\ M_Z \approx 91.19 \text{ GeV}, \quad \sqrt{s} = 5 \text{ TeV}, \quad \mu_f = m_h. \quad (\text{B13})$$

Helicity configuration (λ_A, λ_B)	$\hat{\sigma}$ [pb] (no PDFs)	σ^{LLA} [pb]	σ^{LP} [pb]	σ^{NLP} [pb]
(+, +)	1.693×10^{-3}	119.6×10^{-9}	41.76×10^{-9}	13.56×10^{-9}
(+, -)	150.2×10^{-3}	2960×10^{-9}	1033×10^{-9}	581.2×10^{-9}
(+, 0)	433.3×10^{-6}	41.5×10^{-9}	17.34×10^{-9}	11.13×10^{-9}
(-, +)	150.2×10^{-3}	1351×10^{-9}	471.7×10^{-9}	236.8×10^{-9}
(-, -)	1.693×10^{-3}	119.6×10^{-9}	41.75×10^{-9}	13.56×10^{-9}
(-, 0)	433.3×10^{-6}	31.43×10^{-9}	13.14×10^{-9}	7.715×10^{-9}
(0, +)	433.3×10^{-6}	31.46×10^{-9}	13.15×10^{-9}	7.735×10^{-9}
(0, -)	433.3×10^{-6}	41.44×10^{-9}	17.32×10^{-9}	11.11×10^{-9}
(0, 0)	50.05	1825×10^{-6}	913.0×10^{-6}	817.8×10^{-6}

TABLE IV. Helicity-polarized partonic (column 2) and leptonic (columns 3-5) cross sections [pb] for the $W^+(\lambda_A)W^-(\lambda_B) \rightarrow hh$ sub-process in $\mu^+\mu^-$ collisions at $\sqrt{s} = 5$ TeV, assuming inputs of Eq. (B13), for various W^+W^- helicity configurations (column 1) and LLA/LP/NLP PDFs (column 3/4/5). Partonic cross sections (column 2) use a hard scattering scale of $Q = 1$ TeV.

Appendix C: Scale variation for LP and NLP PDFs

Assuming a collection events, each with cross section weight $\Delta\sigma_k$ with a baseline scale choice $\mu = \mu_0$, then the scale variation of the cross section weight ($\Delta\sigma'_k$) at a scale $\mu = \zeta\mu_0$ is given by the reweighting scheme

$$\Delta\sigma'_k(\zeta\mu_0) = \Delta\sigma_k(\mu_0) \times \frac{w_k(\zeta\mu_0)}{w_k(\mu_0)}. \quad (\text{C1})$$

Here, $w_k(\mu)$ is the scale weight. The scale weight varies according to PDF species and accuracy.

For transverse PDFs at LLA, LP [Eqs. (5b)-(5c)], and NLP [Eqs. (6a)-(6b)], the scale weights are respectively,

$$w_k^{\text{LLA}}(V_{\lambda=\pm}, \mu) = \log\left(\frac{\mu^2}{M_V^2}\right) \quad (\text{C2})$$

$$w_k^{\text{LP}}(V_{\lambda=\pm}, \mu) = \log\left(\frac{M_V^2 + \mu^2}{M_V^2}\right) - \left(\frac{\mu^2}{M_V^2 + \mu^2}\right) \quad (\text{C3})$$

$$w_k^{\text{NLP}}(V_{\lambda=\pm}, \mu) = (a_\lambda + b_T) * \log\left(\frac{M_V^2 + \mu^2}{M_V^2}\right) - \left(\frac{\mu^2}{\mu^2 + M_V^2}\right) * (a_\lambda + c_T), \quad (\text{C4})$$

with coefficients

$$a_{\lambda=+} = (1 - z), \quad a_{\lambda=-} = 1, \quad b_T = (2 - z) \frac{M_V^2}{E_V^2}, \quad (\text{C5})$$

$$c_T = b_T + (2 - z) \frac{\mu^2}{2E_V^2}. \quad (\text{C6})$$

For longitudinal PDFs at LLA, LP [Eq. (5d)], and NLP [Eq. (6c)], the scale weights are respectively,

$$w_k^{\text{LLA}}(V_{\lambda=0}, \mu) = 1 \quad (\text{C7})$$

$$w_k^{\text{LP}}(V_{\lambda=0}, \mu) = \left(\frac{\mu^2}{M_V^2 + \mu^2}\right) \quad (\text{C8})$$

$$w_k^{\text{NLP}}(V_{\lambda=0}, \mu) = \left(\frac{\mu^2}{M_V^2 + \mu^2}\right) - \left\{ \left[\frac{1 - (1 - z)^2}{(1 - z)} \right] \left(\frac{M_V^2}{4E_V^2}\right) \times \left[\log\left(\frac{M_V^2 + \mu^2}{M_V^2}\right) - \left(\frac{\mu^2}{M_V^2 + \mu^2}\right) \right] \right\}. \quad (\text{C9})$$

- [1] E. Witten, Heavy Quark Contributions to Deep Inelastic Scattering, *Nucl. Phys. B* **104**, 445 (1976).
- [2] M. A. G. Aivazis, F. I. Olness, and W.-K. Tung, Leptoproduction of heavy quarks. 1. General formalism and kinematics of charged current and neutral current production processes, *Phys. Rev. D* **50**, 3085 (1994), [arXiv:hep-ph/9312318](#).
- [3] M. A. G. Aivazis, J. C. Collins, F. I. Olness, and W.-K. Tung, Leptoproduction of heavy quarks. 2. A Unified QCD formulation of charged and neutral current pro-

- cesses from fixed target to collider energies, *Phys. Rev. D* **50**, 3102 (1994), [arXiv:hep-ph/9312319](#).
- [4] T. Han, J. Sayre, and S. Westhoff, Top-Quark Initiated Processes at High-Energy Hadron Colliders, *JHEP* **04**, 145, [arXiv:1411.2588 \[hep-ph\]](#).
- [5] S. Dawson, A. Ismail, and I. Low, Redux on ‘‘When is the top quark a parton?’’, *Phys. Rev. D* **90**, 014005 (2014), [arXiv:1405.6211 \[hep-ph\]](#).
- [6] A. D. Martin, R. G. Roberts, W. J. Stirling, and R. S. Thorne, Parton distributions incorporating QED con-

- tributions, *Eur. Phys. J. C* **39**, 155 (2005), [arXiv:hep-ph/0411040](#).
- [7] A. Manohar, P. Nason, G. P. Salam, and G. Zanderighi, How bright is the proton? A precise determination of the photon parton distribution function, *Phys. Rev. Lett.* **117**, 242002 (2016), [arXiv:1607.04266 \[hep-ph\]](#).
- [8] A. V. Manohar, P. Nason, G. P. Salam, and G. Zanderighi, The Photon Content of the Proton, *JHEP* **12**, 046, [arXiv:1708.01256 \[hep-ph\]](#).
- [9] K. Xie, B. Zhou, and T. J. Hobbs (CTEQ-TEA), The photon content of the neutron, *JHEP* **04**, 022, [arXiv:2305.10497 \[hep-ph\]](#).
- [10] S. Dawson, The Effective W Approximation, *Nucl. Phys. B* **249**, 42 (1985).
- [11] G. L. Kane, W. W. Repko, and W. B. Rolnick, The Effective W^+ , Z^0 Approximation for High-Energy Collisions, *Phys. Lett. B* **148**, 367 (1984).
- [12] Z. Kunszt and D. E. Soper, On the Validity of the Effective W Approximation, *Nucl. Phys. B* **296**, 253 (1988).
- [13] M. Ciafaloni, P. Ciafaloni, and D. Comelli, Electroweak Bloch-Nordsieck violation at the TeV scale: 'Strong' weak interactions?, *Nucl. Phys. B* **589**, 359 (2000), [arXiv:hep-ph/0004071](#).
- [14] M. Ciafaloni, P. Ciafaloni, and D. Comelli, Bloch-Nordsieck violating electroweak corrections to inclusive TeV scale hard processes, *Phys. Rev. Lett.* **84**, 4810 (2000), [arXiv:hep-ph/0001142](#).
- [15] M. Ciafaloni, P. Ciafaloni, and D. Comelli, Bloch-Nordsieck violation in spontaneously broken Abelian theories, *Phys. Rev. Lett.* **87**, 211802 (2001), [arXiv:hep-ph/0103315](#).
- [16] P. Ciafaloni and D. Comelli, Electroweak evolution equations, *JHEP* **11**, 022, [arXiv:hep-ph/0505047](#).
- [17] J.-y. Chiu, F. Golf, R. Kelley, and A. V. Manohar, Electroweak Sudakov corrections using effective field theory, *Phys. Rev. Lett.* **100**, 021802 (2008), [arXiv:0709.2377 \[hep-ph\]](#).
- [18] J.-y. Chiu, A. Fuhrer, R. Kelley, and A. V. Manohar, Factorization Structure of Gauge Theory Amplitudes and Application to Hard Scattering Processes at the LHC, *Phys. Rev. D* **80**, 094013 (2009), [arXiv:0909.0012 \[hep-ph\]](#).
- [19] A. Manohar, B. Shotwell, C. Bauer, and S. Turczyk, Non-cancellation of electroweak logarithms in high-energy scattering, *Phys. Lett. B* **740**, 179 (2015), [arXiv:1409.1918 \[hep-ph\]](#).
- [20] J. Chen, T. Han, and B. Tweedie, Electroweak Splitting Functions and High Energy Showering, *JHEP* **11**, 093, [arXiv:1611.00788 \[hep-ph\]](#).
- [21] C. W. Bauer, N. Ferland, and B. R. Webber, Standard Model Parton Distributions at Very High Energies, *JHEP* **08**, 036, [arXiv:1703.08562 \[hep-ph\]](#).
- [22] C. W. Bauer and B. R. Webber, Polarization Effects in Standard Model Parton Distributions at Very High Energies, *JHEP* **03**, 013, [arXiv:1808.08831 \[hep-ph\]](#).
- [23] T. Han, Y. Ma, and K. Xie, High energy leptonic collisions and electroweak parton distribution functions, *Phys. Rev. D* **103**, L031301 (2021), [arXiv:2007.14300 \[hep-ph\]](#).
- [24] S. Frixione and G. Stagnitto, The muon parton distribution functions, *JHEP* **12**, 170, [arXiv:2309.07516 \[hep-ph\]](#).
- [25] J. Lindfors, Distribution Functions for Heavy Vector Bosons Inside Colliding Particle Beams, *Z. Phys. C* **28**, 427 (1985).
- [26] R. Kleiss and W. J. Stirling, Anomalous High-energy Behavior in Boson Fusion, *Phys. Lett. B* **182**, 75 (1986).
- [27] P. W. Johnson, F. I. Olness, and W.-K. Tung, The Effective Vector Boson Method for High-energy Collisions, *Phys. Rev. D* **36**, 291 (1987).
- [28] A. Abbasabadi, W. W. Repko, D. A. Dicus, and R. Vega, Comparison of Exact and Effective Gauge Boson Calculations for Gauge Boson Fusion Processes, *Phys. Rev. D* **38**, 2770 (1988).
- [29] I. Kuss and H. Spiesberger, Luminosities for vector boson - vector boson scattering at high-energy colliders, *Phys. Rev. D* **53**, 6078 (1996), [arXiv:hep-ph/9507204](#).
- [30] I. Kuss, Improved effective vector boson approximation for hadron hadron collisions, *Phys. Rev. D* **55**, 7165 (1997), [arXiv:hep-ph/9608453](#).
- [31] E. Accomando, A. Ballestrero, A. Belhouari, and E. Maina, Isolating Vector Boson Scattering at the LHC: Gauge cancellations and the Equivalent Vector Boson Approximation vs complete calculations, *Phys. Rev. D* **74**, 073010 (2006), [arXiv:hep-ph/0608019](#).
- [32] P. Borel, R. Franceschini, R. Rattazzi, and A. Wulzer, Probing the Scattering of Equivalent Electroweak Bosons, *JHEP* **06**, 122, [arXiv:1202.1904 \[hep-ph\]](#).
- [33] A. Costantini, F. De Lillo, F. Maltoni, L. Mantani, O. Mattelaer, R. Ruiz, and X. Zhao, Vector boson fusion at multi-TeV muon colliders, *JHEP* **09**, 080, [arXiv:2005.10289 \[hep-ph\]](#).
- [34] B. Fuks, J. Neundorff, K. Peters, R. Ruiz, and M. Saimpert, Majorana neutrinos in same-sign $W^\pm W^\pm$ scattering at the LHC: Breaking the TeV barrier, *Phys. Rev. D* **103**, 055005 (2021), [arXiv:2011.02547 \[hep-ph\]](#).
- [35] R. Ruiz, A. Costantini, F. Maltoni, and O. Mattelaer, The Effective Vector Boson Approximation in high-energy muon collisions, *JHEP* **06**, 114, [arXiv:2111.02442 \[hep-ph\]](#).
- [36] A. M. Sirunyan et al. (CMS), Observation of electroweak production of same-sign W boson pairs in the two jet and two same-sign lepton final state in proton-proton collisions at $\sqrt{s} = 13$ TeV, *Phys. Rev. Lett.* **120**, 081801 (2018), [arXiv:1709.05822 \[hep-ex\]](#).
- [37] M. Aaboud et al. (ATLAS), Observation of electroweak production of a same-sign W boson pair in association with two jets in pp collisions at $\sqrt{s} = 13$ TeV with the ATLAS detector, *Phys. Rev. Lett.* **123**, 161801 (2019), [arXiv:1906.03203 \[hep-ex\]](#).
- [38] G. Aad et al. (ATLAS), Measurement and interpretation of same-sign W boson pair production in association with two jets in pp collisions at $\sqrt{s} = 13$ TeV with the ATLAS detector, *JHEP* **04**, 026, [arXiv:2312.00420 \[hep-ex\]](#).
- [39] A. M. Sirunyan et al. (CMS), Measurements of production cross sections of polarized same-sign W boson pairs in association with two jets in proton-proton collisions at $\sqrt{s} = 13$ TeV, *Phys. Lett. B* **812**, 136018 (2021), [arXiv:2009.09429 \[hep-ex\]](#).
- [40] A. Ballestrero et al., Precise predictions for same-sign W -boson scattering at the LHC, *Eur. Phys. J. C* **78**, 671 (2018), [arXiv:1803.07943 \[hep-ph\]](#).
- [41] D. Buarque Franzosi et al., Vector boson scattering processes: Status and prospects, *Rev. Phys.* **8**, 100071 (2022), [arXiv:2106.01393 \[hep-ph\]](#).
- [42] S. Dittmaier, P. Maierhöfer, C. Schwan, and R. Winterhalder, Like-sign W -boson scattering at the LHC — approximations and full next-to-leading-order predictions, *JHEP* **11**, 022, [arXiv:2308.16716 \[hep-ph\]](#).

- [43] B. Henning, D. Lombardo, M. Riemann, and F. Riva, Measuring Higgs Couplings without Higgs Bosons, *Phys. Rev. Lett.* **123**, 181801 (2019), [arXiv:1812.09299 \[hep-ph\]](#).
- [44] R. Bellan et al., A sensitivity study of VBS and diboson WW to dimension-6 EFT operators at the LHC, *JHEP* **05**, 039, [arXiv:2108.03199 \[hep-ph\]](#).
- [45] D. A. Dicus and S. Willenbrock, Higgs Boson Production from Heavy Quark Fusion, *Phys. Rev. D* **39**, 751 (1989).
- [46] F. Maltoni, Z. Sullivan, and S. Willenbrock, Higgs-Boson Production via Bottom-Quark Fusion, *Phys. Rev. D* **67**, 093005 (2003), [arXiv:hep-ph/0301033](#).
- [47] Note that this decoupling of Goldstone bosons, at least at tree level, can possibly soften Bloch-Nordsieck violations [15], i.e., uncancelled infrared EW logarithms.
- [48] W. Bernreuther and L. Chen, Improved effective vector boson approximation revisited, *Phys. Rev. D* **93**, 053018 (2016), [arXiv:1511.07706 \[hep-ph\]](#).
- [49] M. E. Peskin and D. V. Schroeder, [An Introduction to quantum field theory](#) (Addison-Wesley, Reading, USA, 1995).
- [50] H. Georgi and H. D. Politzer, Precocious Scaling, Rescaling and xi Scaling, *Phys. Rev. Lett.* **36**, 1281 (1976), [Erratum: *Phys.Rev.Lett.* 37, 68 (1976)].
- [51] H. Georgi and H. D. Politzer, Freedom at Moderate Energies: Masses in Color Dynamics, *Phys. Rev. D* **14**, 1829 (1976).
- [52] G. Altarelli, B. Mele, and F. Pitolli, Heavy Higgs Production at Future Colliders, *Nucl. Phys. B* **287**, 205 (1987).
- [53] R. P. Kauffman, Production of Top Quarks via Vector Boson Fusion in e^+e^- Collisions, *Phys. Rev. D* **41**, 3343 (1990).
- [54] S. Frixione, M. L. Mangano, P. Nason, and G. Ridolfi, Improving the Weizsacker-Williams approximation in electron - proton collisions, *Phys. Lett. B* **319**, 339 (1993), [arXiv:hep-ph/9310350](#).
- [55] C. Dams and R. Kleiss, The Electroweak standard model in the axial gauge, *Eur. Phys. J. C* **34**, 419 (2004), [arXiv:hep-ph/0401136](#).
- [56] J. Chen, On the Feynman Rules of Massive Gauge Theory in Physical Gauges, (2019), [arXiv:1902.06738 \[hep-ph\]](#).
- [57] J. Chen, K. Hagiwara, J. Kanzaki, and K. Mawatari, Helicity amplitudes without gauge cancellation for electroweak processes, *Eur. Phys. J. C* **83**, 922 (2023), [Erratum: *Eur.Phys.J.C* 84, 97 (2024)], [arXiv:2203.10440 \[hep-ph\]](#).
- [58] J. Chen, K. Hagiwara, J. Kanzaki, K. Mawatari, and Y.-J. Zheng, Helicity amplitudes in light-cone and Feynman-diagram gauges, *Eur. Phys. J. Plus* **139**, 332 (2024), [arXiv:2211.14562 \[hep-ph\]](#).
- [59] K. M. Black et al., Muon Collider Forum report, *JINST* **19** (02), T02015, [arXiv:2209.01318 \[hep-ex\]](#).
- [60] S. Asai et al. (P5), Exploring the Quantum Universe: Pathways to Innovation and Discovery in Particle Physics [10.2172/2368847](#) (2023), [arXiv:2407.19176 \[hep-ex\]](#).
- [61] C. Accettura et al., Towards a muon collider, *Eur. Phys. J. C* **83**, 864 (2023), [Erratum: *Eur.Phys.J.C* 84, 36 (2024)], [arXiv:2303.08533 \[physics.acc-ph\]](#).
- [62] D. Buarque Franzosi, O. Mattelaer, R. Ruiz, and S. Shil, Automated predictions from polarized matrix elements, *JHEP* **04**, 082, [arXiv:1912.01725 \[hep-ph\]](#).
- [63] T. Stelzer and W. F. Long, Automatic generation of tree level helicity amplitudes, *Comput. Phys. Commun.* **81**, 357 (1994), [arXiv:hep-ph/9401258](#).
- [64] J. Alwall, R. Frederix, S. Frixione, V. Hirschi, F. Maltoni, O. Mattelaer, H. S. Shao, T. Stelzer, P. Torrielli, and M. Zaro, The automated computation of tree-level and next-to-leading order differential cross sections, and their matching to parton shower simulations, *JHEP* **07**, 079, [arXiv:1405.0301 \[hep-ph\]](#).
- [65] J. C. Collins, D. E. Soper, and G. F. Sterman, Transverse Momentum Distribution in Drell-Yan Pair and W and Z Boson Production, *Nucl. Phys. B* **250**, 199 (1985).
- [66] H. Contopanagos, E. Laenen, and G. F. Sterman, Sudakov factorization and resummation, *Nucl. Phys. B* **484**, 303 (1997), [arXiv:hep-ph/9604313](#).
- [67] V. Ahrens, T. Becher, M. Neubert, and L. L. Yang, Renormalization-Group Improved Prediction for Higgs Production at Hadron Colliders, *Eur. Phys. J. C* **62**, 333 (2009), [arXiv:0809.4283 \[hep-ph\]](#).
- [68] T. Becher, A. Broggio, and A. Ferroglia, [Introduction to Soft-Collinear Effective Theory](#), Vol. 896 (Springer, 2015) [arXiv:1410.1892 \[hep-ph\]](#).